Molecular Therapy
Original Article

Long-term effects of s-KL treatment in wild-type mice: Enhancing longevity, physical well-being, and neurological resilience

Joan Roig-Soriano,[1,2] Ángel Edo,[1,2] Sergi Verdés,[1,2] Carlos Martín-Alonso,[1] Cristina Sánchez-de-Diego,[2] Laura Rodriguez-Estevez,[1,2] Antonio L. Serrano,[7,10] Carmela R. Abraham,[5] Assumpció Bosch,[1,2,6] Francesc Ventura,[3] Bryen A. Jordan,[4] Pura Muñoz-Cánoves,[7,8,10] and Miguel Chillón[1,2,8,9]

[1]Institut de Neurociències (INc), Universitat Autònoma de Barcelona, 08193 Bellaterra, Spain; [2]Vall d'Hebron Institut de Recerca (VHIR), 08035 Barcelona, Spain; [3]IDIBELL, Universitat de Barcelona, 08908 Barcelona, Spain; [4]Dominick P. Purpura Department of Neuroscience, Albert Einstein College of Medicine, New York, NY 10461, USA; [5]ADvantage Therapeutics, Inc., Miami, FL 33127, USA; [6]Ciberned, Instituto de Salud Carlos III, 28029 Madrid, Spain; [7]Department of Medicine and Life Sciences, Pompeu Fabra University, 08003 Barcelona, Spain; [8]ICREA, 08010 Barcelona, Spain; [9]Unitat de Producció de Vectors (UPV), Universitat Autònoma de Barcelona, 08193 Barcelona, Spain; [10]Altos Labs, San Diego Institute of Science, San Diego, CA 92122, USA

Aging is a major risk factor for pathologies including sarcopenia, osteoporosis, and cognitive decline, which bring suffering, disability, and elevated economic and social costs. Therefore, new therapies are needed to achieve healthy aging. The protein Klotho (KL) has emerged as a promising anti-aging molecule due to its pleiotropic actions modulating insulin, insulin-like growth factor-1, and *Wnt* signaling pathways and reducing inflammatory and oxidative stress. Here, we explored the anti-aging potential of the secreted isoform of this protein on the non-pathological aging progression of wild-type mice. The delivery of an adeno-associated virus serotype 9 (AAV9) coding for secreted KL (s-KL) efficiently increased the concentration of s-KL in serum, resulting in a 20% increase in lifespan. Notably, KL treatment improved physical fitness, related to a reduction in muscle fibrosis and an increase in muscular regenerative capacity. KL treatment also improved bone microstructural parameters associated with osteoporosis. Finally, s-KL-treated mice exhibited increased cellular markers of adult neurogenesis and immune response, with transcriptomic analysis revealing induced phagocytosis and immune cell activity in the aged hippocampus. These results show the potential of elevating s-KL expression to simultaneously reduce the age-associated degeneration in multiple organs, increasing both life and health span.

INTRODUCTION

Progress in health care and quality of life in modern societies have led to an increase in the percentage of the population reaching advanced ages, with a projected 25% of citizens in developed countries being over the age of 65 by 2060.[1] Aging is the main risk factor for a wide range of pathologies that lead to the progressive decline of organ and tissue functions. Among the most affected systems during aging are the locomotor nervous system and the CNS, significantly impacting the health span and autonomy of aged individuals.[2]

Muscle aging is primarily marked by sarcopenia, known as the progressive loss of muscular fibers and the total muscle volume. This is one of the main causes of the increased weakness observed during aging, although metabolic, cellular, and neuromuscular alterations are also involved.[3] Non-pathological aging results in an estimated 3%–8% loss of total muscular mass per decade, starting around age 30.[4] This is associated with anatomical changes in muscular cells and reduced muscular protein production, limiting tissue regeneration.[5,6] Moreover, satellite cells, quiescent stem cells in muscles, lose functionality during aging, reducing muscle regenerative capacity.[7] Consequently, there is a decrease in muscular tissue and a progressive accumulation of fatty and fibrotic tissues that reduce the functionality of muscles.[8]

Osteoporosis, together with sarcopenia, is a clear contributor to the increased frailty observed in the elderly. It is understood as a reduction in bone tissue density and mass, affecting both the cortical and the trabecular bone. Additionally, the shape and structure of these bone components are also altered during aging.[9,10] The main changes observed during osteoporosis progression include a decrease in trabecular bone caused by thinning and structural loss of the trabeculae.[9,11] Moreover, there is a progressive endocortical bone resorption, which increases the luminary volume within bones from 25% to 40% during aging.[12] Furthermore, there is a loss in bone mineral density, as a result of both the increased bone resorption, carried out by osteoclast cells, and the reduction in bone formation due to

Received 21 March 2024; accepted 19 February 2025;
https://doi.org/10.1016/j.ymthe.2025.02.030.

Correspondence: Miguel Chillón, Institut de Neurociències (INc), Universitat Autònoma de Barcelona, 08193 Bellaterra, Spain.
E-mail: miguel.chillon@uab.es

altered osteoblast differentiation and function.[12] Finally, the expression of collagen and non-collagenous bone proteins is also altered during aging. These alterations impact the physical properties and chemical composition of bones, contributing to the development of osteoporosis.[13]

Aging progression in the CNS varies between individuals, with some experiencing healthy aging and others developing neurodegenerative diseases like Alzheimer's or Parkinson's diseases.[14] Mature neurons do not proliferate, and adult neurogenesis occurs only in specific regions, although this process is progressively reduced during adulthood.[15] Hence, stressor factors accumulate during aging and generate a progressive loss of neuronal cells and synaptic connections, significantly decreasing neuronal plasticity.[16] Additionally, glial cells are also altered during aging, with changes in the number, morphology and function of microglia and astrocyte cells, hindering their function.[17,18] For instance, these cells can become chronically activated, thus promoting inflammatory and oxidative stress in neurons.[19] Moreover, microglia reduce their capacity to migrate to damaged areas and to phagocytose malfunctioning elements.[20] These progressive modifications can be assessed and quantified, representing helpful markers to study the fitness of the brain and the efficacy of neurodegeneration-protective factors.

In this context, the protein Klotho (KL) has been identified as a promising anti-aging molecule due to its pleiotropic actions on pathways regulating longevity. KL gene presents two main transcripts. The full-length mRNA generates a transmembrane protein, known as m-KL, composed of an extracellular portion containing two homologous domains, KL1 and KL2.[21,22] These extracellular components can later be shed from the membrane through an enzyme-dependent mechanism, resulting in the complete soluble form known as p-KL, or the individual domains p-KL1 and p-KL2. Alternatively, the shorter transcript presents a premature stop codon and generates a secreted isoform, known as s-KL. This isoform contains the KL1 domain with an additional C-terminal tail of 14 amino acid specific of s-KL (SPLTKPSVGLLLPH).[23] The transmembrane protein is an obligate co-receptor for fibroblast growth factor-23 (FGF23), being a key component for mineral metabolism regulation.[24,25] Soluble and secreted KL (s-KL) isoforms present anti-aging properties by reducing cellular inflammatory and oxidative stress, as well as modulating several signaling pathways involved in senescence like *Wnt*, insulin, and insulin-like growth factor-1 pathways.[26] Previous reports have demonstrated beneficial effects against age-associated deficits from expressing different KL isoforms, despite their significantly different pharmacological profiles. While s-KL has shown a safe profile, the p-KL isoform interferes with mineral metabolism regulation, thereby raising safety concerns.[27] Therefore, here we analyze the potential therapeutic effects against age-associated degeneration of the safer s-KL isoform.

Age-associated deficits develop gradually over long periods of time, frequently not associated with pathologies. Thus, we assess the effects of long-term expression of s-KL over the evolution of non-pathological aging hallmarks, especially those generating elevated rates of dependence during human aging, such as muscular and bone fitness, neuronal degeneration, and total longevity.

RESULTS

Long-term expression of s-KL increases median and total longevity in male mice

To study the effects of s-KL over the progression of aging phenotype and longevity of wild-type mice, we generated adeno-associated virus serotype 9 (AAV9) gene therapy vectors expressing s-KL or a non-transcribing/null control sequence. AAV9 vectors were delivered through a combination of intracerebroventricular (ICV) and intravenous (IV) (tail vein) injections, enabling efficient transduction of both the CNS and peripheral tissues. Two time points for treatment administration were set, establishing three experimental groups. Two groups were treated in a young-adult developmental stage, when animals were 6 months old (MO), with a control (null 6 MO group) or a murine s-KL-expressing AAV9 (s-KL 6 MO group). The third group was treated with an s-KL-expressing vector when animals were 12 MO (s-KL 12 MO group). Although most of the animals were allowed to age to measure total lifespan, a randomly selected subset of animals of each group were euthanized at 24 months of age to assess viral vector function and study aging progression in treated animals (Figure 1A).

Treated animals were periodically examined to assess their aging phenotype evolution. In males, mean body weight peaked at the age of 14 months for null, 15 months for s-KL 6 MO, and at 20 months of age for the s-KL 12 MO group (Figure 1B). As shown in Figure 1C, the median survival in males was of 24.6, 25.8, and 28.3 months for the null-treated, sKL-6 MO, and sKL-12 MO groups, respectively, representing a statistically significant increase of 15% in life expectancy of s-KL 12 MO compared with null-treated animals. The total longevity of the different groups is presented in Kaplan-Meier survival curves (Figure 1D), being 26.3, 29.8, and 31.5 months for the null-treated, s-KL 6 MO, and s-KL 12 MO groups, respectively. This result represents a 19.7% increase in total longevity in the s-KL 12 MO group, which is statistically significant at p value of 0.005 using the Mantel-Cox statistical test (null 6 MO compared with s-KL 12 MO). In contrast, follow-up of female groups revealed a high incidence of ulcerative dermatitis and anal bleeding. These health problems occurred at different time points of the longevity follow-up and required animal euthanasia. Due to the uneven distribution of these conditions among groups and the possibility that they were not age associated, we could not consider longevity data obtained for females.

In parallel, a subset of animals from the null 6 MO, s-KL 6 MO, and s-KL 12 MO groups were euthanized when animals were 24 MO, that is, at 18, 18, and 12 months after the treatment, respectively. These samples were used to study AAV treatment efficacy and aging progression in different organs. Expression of the s-KL cDNA in the liver (Figure 1E) and KL protein concentration in serum (Figure 1F)

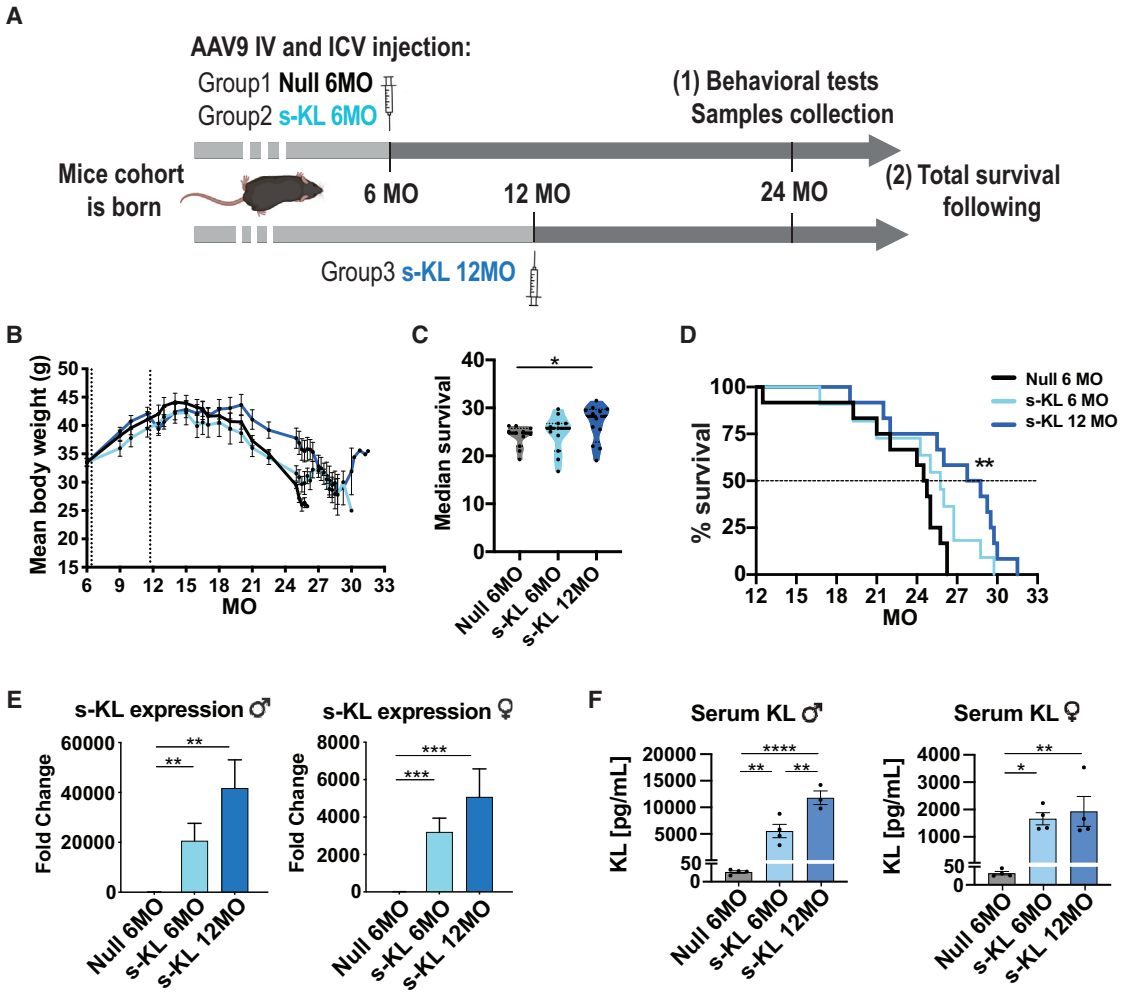

Figure 1. Longevity experiment follow-up and AAV treatment effectivity assessment

(A) Schematic representation of the experimental plan. AAV9, IV, and ICV. (B) Body weight follow-up. (C) Violin plots of the median survival of the different treatments tested in males. (D) Longevity of the different male groups represented with Kaplan-Meyer longevity curves. Mean ± SEM, $n = 11–12$. (E) Schematic representation of the experimental plan. (F) s-KL gene expression analysis in the liver. Data presented as fold change expression compared with null-treated animals. (G) Quantification of total s-KL protein concentration in serum. Data presented as mean ± SEM, $n = 4$; $^{*}p < 0.05$; $^{**}p < 0.01$; $^{***}p < 0.001$; $^{****}p < 0.001$.

were significantly increased in KL-treated groups. Of note, gene expression and protein concentration were higher in male than in female groups, and in the 12 MO group compared with the 6 MO-treated animals.

Mice treated with s-KL improved physical state and reduced muscular fibrosis

A battery of behavioral tests was conducted when animals were 24 MO to assess the physical state progression across the different groups. As observed in Figure 2A, s-KL-treated females displayed improved performance in rotarod testing, both when treated at 6 and 12 MO. Moreover, both males and females improved horizontal bar performance, reaching statistical significance for the s-KL-treated animals at 12 months of age (Figure 2B). Finally, an improvement in grip strength was observed for s-KL-treated males. In this case, s-KL-treated females also performed significantly better in the first trial of the test, but these differences were not observed for the second and third trials (Figure 2C).

Soleus muscle from aged animals (24 MO) was studied using hematoxylin and eosin staining to assess muscle fibers size and with Sirius red staining to quantify the percentage of muscle fibrotic tissue. As seen in Figure 2D, males treated with s-KL exhibited an average increase in soleus muscle fiber size of 20% compared with null-treated mice, although these differences did not a statistical significance. In contrast, there was a significant and consistent reduction in the presence of fibrosis in the muscles of male mice treated with s-KL at the age of 12 MO (Figure 2E).

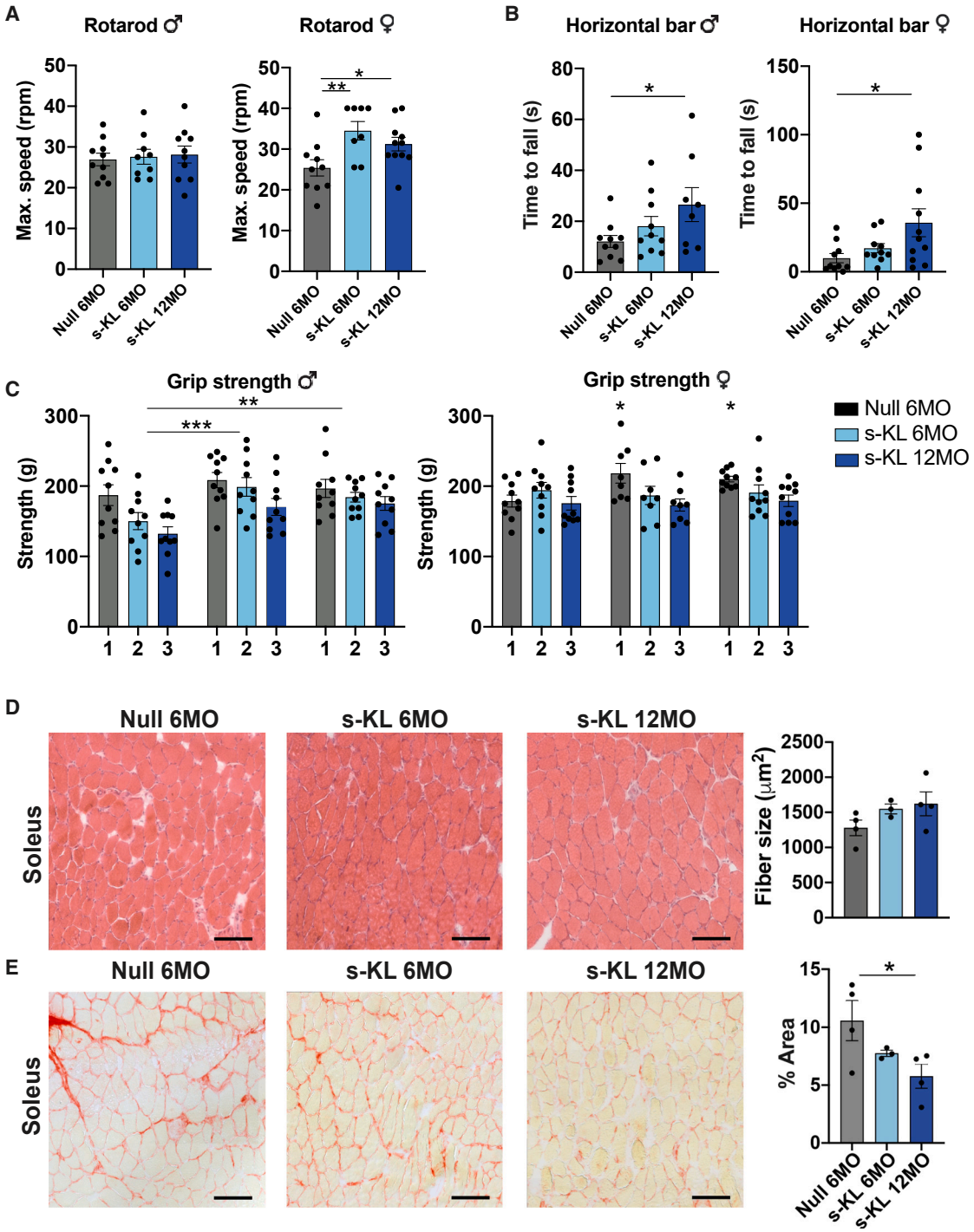

Figure 2. Physical tests and histological analysis of muscular tissue from treated naturally aged animals

(A) Results of the accelerating rotarod test, showed as the maximum speed at which the animals were able to run. (B) Results of horizontal bar test, presented as time animals held on the bar. (C) Results of grip strength test, presented as the average force that each group exhibit in the three trials done. Data presented as mean ± SEM, $n = 8–11$; $^{*}p < 0.05$; $^{**}p < 0.01$; $^{***}p < 0.001$. (D) Hematoxylin and eosin staining of fibers of the soleus muscle of male mice. Fiber size was quantified and the average size per animal was presented. (E) Sirius red staining of the soleus muscles. Graphs present the percentage of fibrotic area present in each sample. Scale bar, 100 μm. Data presented as mean ± SEM, $n = 4$; $^{*}p < 0.05$; $^{**}p < 0.01$.

s-KL improved the regenerative capacity of aged muscles

Muscular regenerative capacity is highly reduced with aging. Whole muscle transplantation from aged animals into naive young recipients induces tissue degeneration and subsequent regeneration of the transplanted muscles within a young systemic environment. Thus, the regenerative capacity of muscles from 24-MO treated animals was assessed after transplantation of the extensor digitorum longus muscle into young mice receivers. One week after engraftment, the number and size of the fibers regenerating in the muscular graft were quantified (Figure 3A). Compared with null-treated muscles, animals that received the s-KL treatment at 6 MO showed increased average size of myofibers present in the graft. In addition, s-KL treatment at 12 MO also increased the percentage of bigger regenerating fibers, indicating an improvement of the regenerative capacity (Figures 3B and 3C).

We next analyzed the presence of several regeneration-related markers in the grafts. An increase in the number of cells co-expressing the cellular proliferation marker Ki67 and PAX7, a marker of satellite cells (responsible for muscular regeneration), was detected (Figure 3D). Moreover, the number of cells expressing the myogenic regulatory factor MyoD, a marker of myogenic commitment of muscular satellite cells, was also significantly increased in the grafts of s-KL-treated animals (Figure 3D).

Bone tissue from animals treated with s-KL presented improved trabecular variables and increased expression of bone morphogenic proteins

Analysis of the microstructure of bones from aged animals showed structural improvements in different variables, mainly associated with the trabecular bone. These effects were specifically observed in female mice treated at 6 months of age, and tendencies in males treated with s-KL at 12 months of age. Changes included an increase in trabecular bone volume, trabecular number and thickness, and a reduction of the trabecular space (Figures 4A and 4B).

AAV9 efficiently transduced cells in bone tissue, with s-KL expression significantly increased in all s-KL-treated groups compared with control null-treated animals. Specifically, s-KL expression in treated males compared with null was increased by 73.3 ± 32.6 SEM (n = 5) and 287.2 ± 96.2 SEM (n = 6) in s-KL 6 MO and 12 MO, respectively, while in females, s-KL expression was increased by 185 ± 45.8 SEM (n = 6) and 161.2 ± 56.6 SEM (n = 4) in s-KL 6 MO and 12 MO, respectively. Interestingly, the expression of bone morphogenic genes was increased in treated animals, especially in females (Figure 4C). The *Bglap* gene, which encodes for a protein involved in calcium accumulation in bones and represents a marker for bone formation, increased its expression in both s-KL-treated female groups. Moreover, the collagen type 1 gene (*Col1a1*), which is the main organic component of the bone, tended to increase in 6 MO s-KL-treated females (p = 0.06). RNA expression analysis of gene makers for different bone cell lineages presented high variability. Despite that, a significant increase in the expression of the osteoblast gene *Runx2,* and a decrease in *Fgf23* gene expression was observed in s-KL-treated females.

Effect of the s-KL expression on hippocampal histological markers altered by aging

Histological analysis of the CNS of treated male and female mice showed that s-KL treatment increased several cellular markers important for the correct function of the CNS. Specifically, in different areas of the hippocampus, an increase in the percentage of stained area and the number of $Iba1^+$ cells was observed in 12 MO s-KL-treated animals (Figure 5A). Additionally, these variables also increased for the GFAP marker in animals treated with s-KL at both 6 MO and 12 MO (Figure 5B). To better understand this effect, young mice (3 MO) were treated with AAV expressing s-KL or a null sequence. Two months after the treatment, no changes were observed in the number or the percentage of stained area of GFAP or IBA1 markers in young animals (Figures S1A and S1B).

As previously mentioned, adult neurogenesis is highly decreased either during aging or under stressor factors, correlating with CNS fitness. Histological analysis of aged animals treated at 12 months of age (s-KL 12 MO) showed a greater number of maturating neurons (DCX^+ cells) and a tendency to an increase in the average thickness of the granular cells layer of the dentate gyrus, compared with null-treated mice (Figure 5C). To further explore this effect, neurogenesis was also assessed in treated young mice. In this case, a significant increase in $Ki67^+$ cells and DCX^+ cells was observed in s-KL-treated animals (Figure S1C).

s-KL expression regulated the transcriptomic profile of the hippocampus

The mRNA expression profile of the hippocampus from treated mice was analyzed to assess the transcriptional changes during non-pathological aging and after long-term exogenous s-KL expression. For this, total mRNA from the hippocampus of young animals (5 MO), old animals (24 MO) treated with null AAV9 vectors, and old animals (24 MO) treated with s-KL AAV9 at the age of 12 months, was sequenced. Bioinformatic analysis showed that these samples clustered into three different populations based on principal components of variance, suggesting characteristic expression profiles (Figure 6A).

Next, transcription levels of every gene were compared with obtain the differentially expressed genes (DEGs) between the three groups (adjusted $p < 0.05$). As seen in Figure 6B, 3,131 genes were differentially expressed during non-pathological aging (old vs. young null animals), 964 genes were altered during aging of animals treated with s-KL (old s-KL vs. null young animals), and 184 genes differed between old animals treated with null and s-KL AAVs (old s-KL vs. old null animals). Thus, aged animals treated with s-KL presented fewer altered genes than null-treated animals, compared with young mice. Notably, we confirmed KL gene expression was significantly increased in the hippocampus of s-KL-treated mice. Normalized counts of KL gene in RNA sequencing (RNA-seq) data showed a 10-fold and 18-fold increase in s-KL 6 MO and 12 MO mice, respectively, compared with null-treated mice. Specifically, normalized raw counts were 2,450 ± 984.5 SEM (n = 5), 24,477 ± 11,211 SEM (n = 5), and 43,909 ± 16,377 SEM (n = 4), null 6 MO, s-KL 6 MO, and s-KL 12

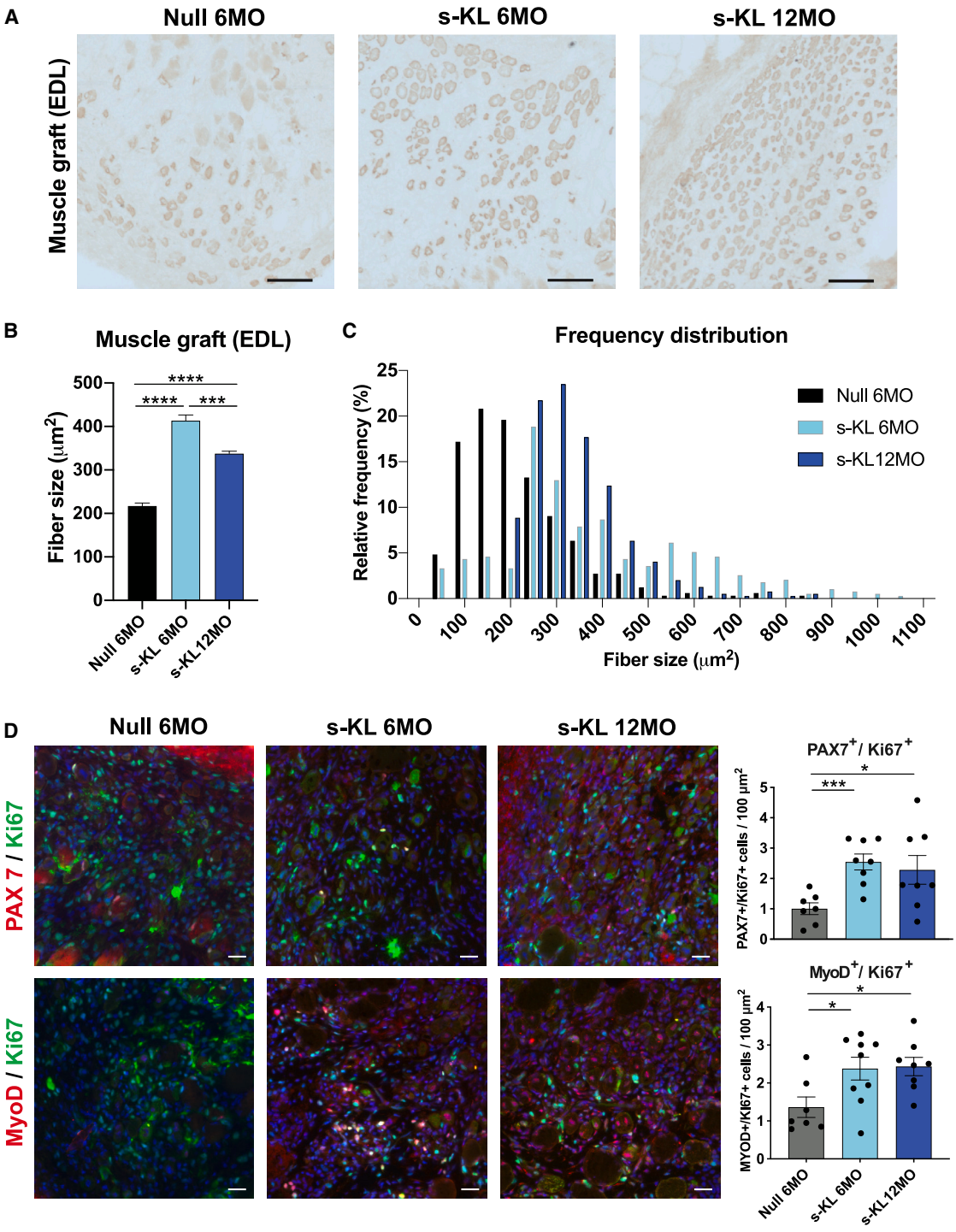

Figure 3. Histological analysis of muscle from s-KL-treated animals 7 days after transplantation

(A) Representative images of grafted muscular tissue stained for embryonic myosin heavy-chain by immunohistochemistry. Scale bar, 100 µm. (B) Quantification of muscular fibers presented as average fiber size and (C) frequency of the different fiber sizes. (D) Quantification of double PAX7 and Ki67 positive cells (first row) and double MyoD and Ki67 positive cells (second row) found in the grafts. Scale bars, 25 µm. Data presented as mean ± SEM, n = 8–9 (males and females); *$p < 0.05$; **$p < 0.01$; ***$p < 0.001$.

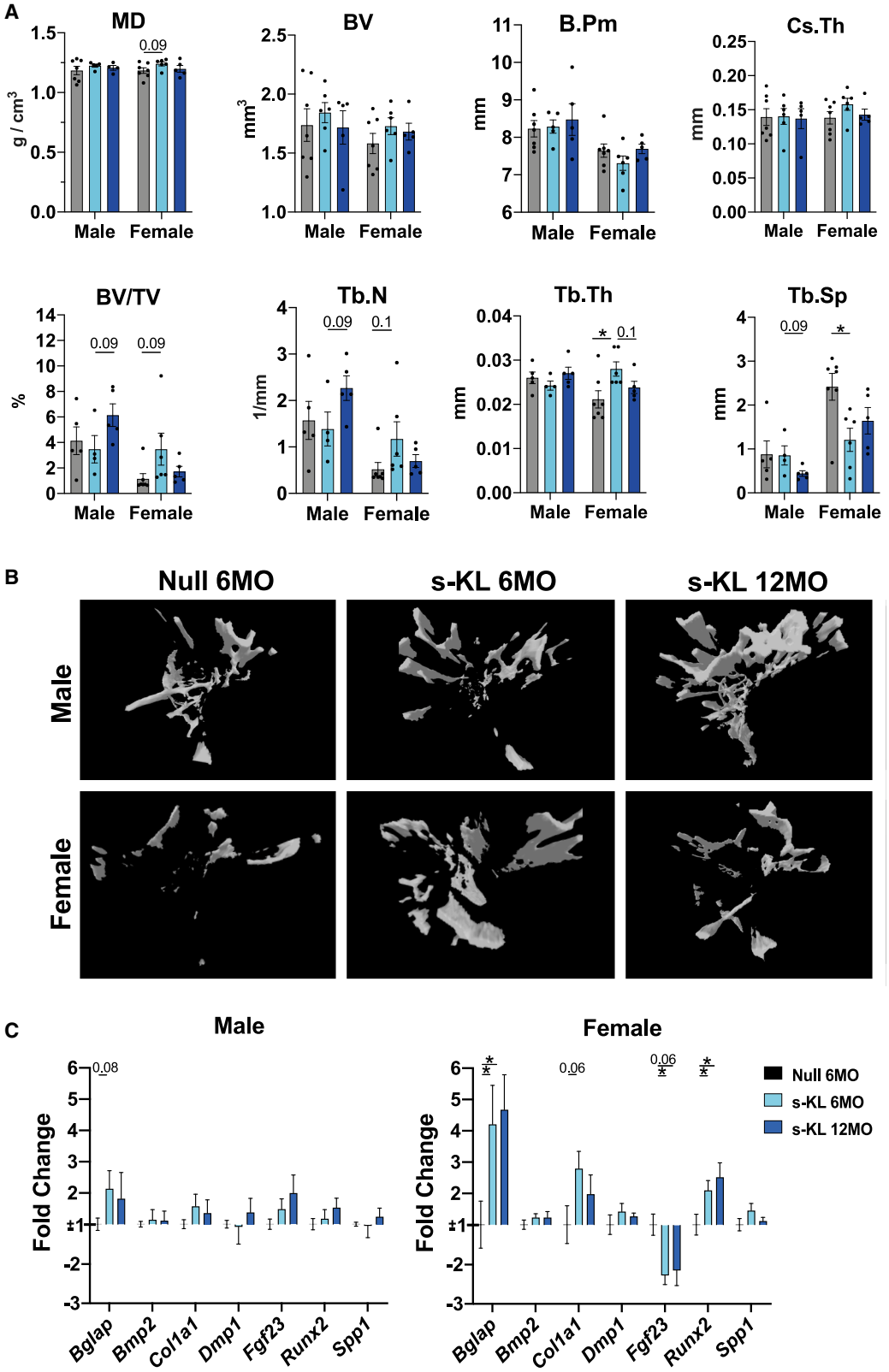

(legend on next page)

MO mice, respectively. Interestingly, expression of s-KL induced specific transcriptional changes in aged animals, as revealed by an ingenuity pathway analysis. This analysis considers all the DEGs and identifies alterations in specific metabolic pathways, showing the biological implication of the transcriptional changes. As can be seen in Table S1, in control null-treated animals, aging was associated with a decrease in oxidative phosphorylation and an increase in mitochondrial dysfunction, as the most downregulated and upregulated canonical pathways. In contrast, animals expressing high levels of s-KL during aging did not present alterations in those pathways. In this case, pathways altered in aged animals treated with s-KL compared with young mice involved the activation of immune cells and the promotion of immune cell activity in the hippocampus (Table S2). Finally, a comparison was made between the transcriptomic state of aged individuals treated with null or s-KL. Compared with aged null-treated mice, long-term s-KL-treated animals presented increased induction of phagocytosis and increased immune cell activation, but accompanied by a decrease in pro-inflammatory signals induction (increase in interleukin [IL]-10 and decrease in IL-12 signaling) (Figure 6C). The molecular alterations responsible for these changes are shown in the schematic representation in Figure 6D.

DISCUSSION

KL protein has been described as a powerful anti-aging molecule, presenting promising results for developing therapies against age-associated degeneration. In this context, there is a need to better understand the long-term effects of the expression of this protein, especially of the s-KL isoform, which presents a safe pharmacological profile.[27] Here, we used gene therapy vectors as a proof of principle to increase s-KL concentration, as it allows constant long-term transcript expression requiring just a single administration. This strategy is convenient for experiments involving senescent animals, thereby reducing their handling and stress.[28–31] We used the AAV9 serotype to efficiently transduce key tissues affected by aging, such as bone, muscle, liver, and the CNS.[32] Since the KL protective effect was needed systemically but also in the nervous system, and KL seems to not cross the blood-brain barrier, we performed both IV and ICV injections.[33–35] In this regard, the double injection approach could be avoided in future studies using AAV serotypes with enhanced capacity to cross the blood-brain barrier following IV injection, increasing translatability to the clinic.[36] Finally, our objective was to achieve a strong ubiquitous expression of the transgene, so we selected the ubiquitous CAG promoter.[37]

This experimental design allowed robust and long-lasting expression of s-KL in treated mice at both young adult (6 MO) or adult (12 MO) administration points, periods equivalent to the developmental stages of an adult human (20–25 years) or middle-aged human (38–47 years), respectively.[38,39] Of note, at the endpoint of the experiment (24 MO), a difference was observed in s-KL protein level production between the s-KL 6 MO and s-KL 12 MO groups. These differences might be attributed to the progressive loss of viral genomes in the liver of animals treated at 6 MO due to cell renewal occurring during the 6 months between the two AAV administration points.[40] Moreover, adult female mice presented lower s-KL expression and protein levels compared with male mice. These differences agree with previous results that show decreased transgene expression in the liver of females after an AAV treatment.[41]

An s-KL-based treatment for aging has the potential to simultaneously modulate several senescence hallmarks, which represents a multifactorial approach against aging decline. Remarkably, male mice treated with s-KL increased both median and total longevity in both the s-KL 6 MO and s-KL 12 MO groups. Despite the experimental groups consisting of 11–12 animals, the results are sufficiently robust to detect statistically significant differences in the group treated when animals were adults (12 MO). We hypothesize that differences in significance observed between the longevity effects in the s-KL groups treated at different time points might be associated with the increased protein concentration observed in the s-KL 12 MO group, rather than being determined by the moment when the treatment was administered. In contrast, for female mice, it was not possible to draw conclusions regarding longevity results due to the high incidence of ulcerative dermatitis and anal prolapse/bleeding in all experimental groups.[42] For this reason, to address s-KL effects on female longevity, it would be necessary to conduct tests in a different genetic background. Previous data had linked increased KL expression with increased longevity, although it was observed in different transgenic KL-overexpressing mouse models or associated with different KL gene variants.[43,44] In contrast, this is the first time that a single treatment of AAVs expressing s-KL significantly increases the longevity of healthy wild-type mice.

Certainly, anti-aging treatments should not only increase longevity but also extend health span promoting healthy aging. Therefore, to study s-KL effects over the progression of age-associated degeneration, different behavioral tests and histological parameters were assessed in treated mice at the age of 24 months. This time point was chosen as, at 24 months, aging progression has already induced an evident physical and cognitive decline in wild-type mice.[38]

We observed that the s-KL treatment promoted an improvement in physical capacities in different tests. Compared with null animals, s-KL-treated mice presented increased resistance in the horizontal bar, especially when treated at 12 MO, which is associated

Figure 4. MicroCT structural and gene expression analysis in treated bones of 24-MO mice

(A) Micro-computed tomography (MicroCT) analysis of different structural variables. Cortical bone: BV, bone volume), B.Pm, bone perimeter; CsTh, cross-sectional thickness; MD, mineral density. Trabecular bone: BV/TV ratio, bone volume/tissue volume; Tb.N, trabecular number; Tb.Th, trabecular thickness; Tb.Sp, trabecular space. (B) Bone reconstruction of the regions of interest analyzed. (C) Effect of the s-KL treatment on the expression of genes representative of the different bone cell types, and bone morphogenic and bone matrix proteins. Data presented as fold change expression compared with null-treated animals. Mean ± SEM, $n = 4–7$; $^{*}p < 0.05$; $^{**}p < 0.01$.

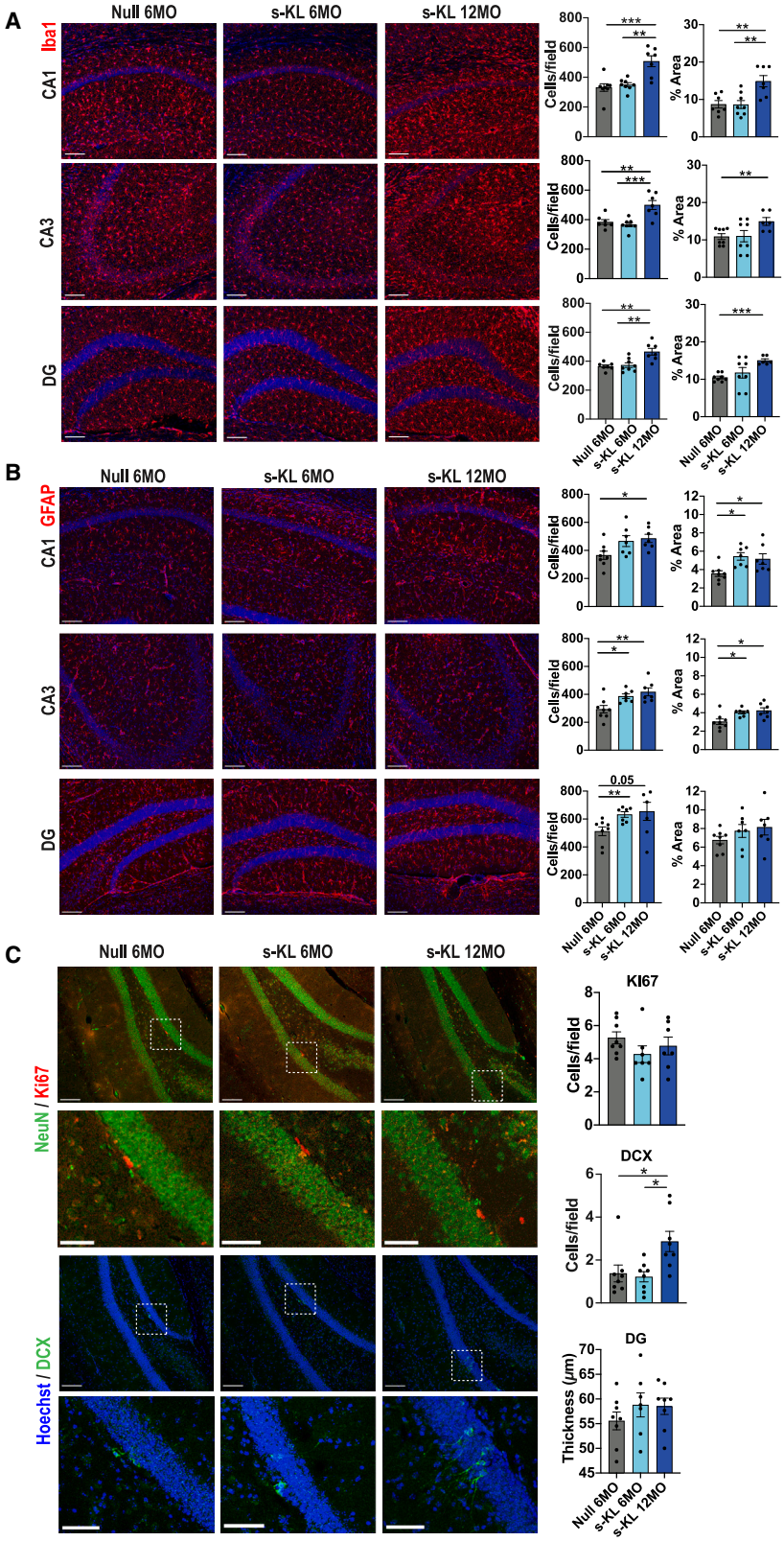

Figure 5. Histological analysis of Iba1, GFAP, and neurogenesis markers in CNS from aged animals

(A) Immunofluorescence analysis of brain slices for Iba1 (A) and GFAP (B) markers in the CA1, CA3 and dentate gyrus (DG) of the hippocampus. Scale bar, 100 μm. Value measured as average number of cells per slide (first graph) and percentage of positively stained area per image (second graph). (C) Quantification of markers representative of different differentiation stages of neurons. Cell proliferation marker (neuronal stem cells) (Ki67 in red), immature neurons (DCX in green), and mature neurons (NeuN) in green. Value measured as average number of cells per slide, or as thickness. Scale bar for images, 100 μm (first and third row) and 50 μm (second and fourth row). Each brain area was analyzed at least at three different anteroposterior positions, and in duplicate. Mean ± SEM, n = 7–8 (males and females).

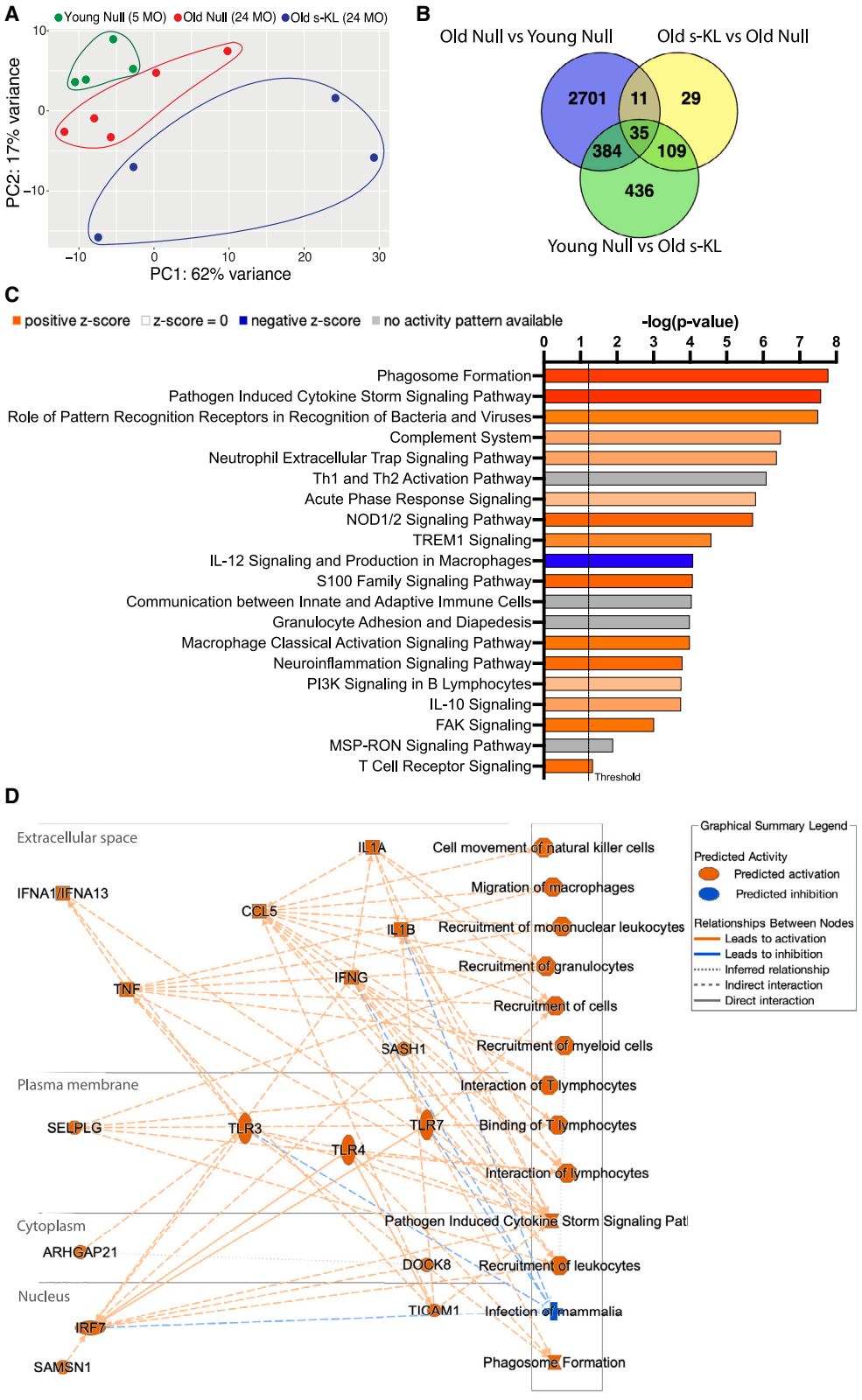

(legend on next page)

with increased muscular resistance and coordination. Furthermore, gender-specific improvements were also detected: females showed improved coordination in the rotarod test, while males exhibited increased strength in the grip strength test. These tests measure motor coordination and balance, and maximum grip muscle strength, respectively, parameters that are altered during the progression of aging.[45] Differences observed between genders could be related to peculiarities in body weight and muscular physiology between males and females, as well as sex-specific characteristics in muscle degeneration progression.[46]

Histological analysis of the muscle tissue of s-KL-treated mice revealed a tendency to an increased size of muscular fibers in aged tissue compared with null-treated mice. Previous reports have shown that strong muscular degeneration in mice becomes prominent after the age of 24 months[47–49]; therefore, in our samples from 24-MO animals the degeneration might be yet incipient to be able to observe an effect of s-KL over this variable. In addition, increasing the sample size for this analysis ($n = 3–4$) may provide a clearer view of the effects of s-KL on muscle fiber preservation during aging. In contrast, a significant reduction in the percentage of fibrotic tissue was observed in samples of 24 MO males treated at 12 months of age. This could explain why this group performed better than null 6 MO and s-KL 6 MO in tests implying resistance, like the horizontal bar test, both in males and females. These results are comparable with those from Clemens et al.,[49] who reported reduced muscular fibrosis in old muscles treated with full-length KL. During aging, muscular fibrosis is induced by the presence of senescent cells, which inhibit proper muscular regeneration by secreting pro-inflammatory and pro-fibrotic molecules.[50] Interestingly, KL has been shown to inhibit pro-fibrotic molecules like transforming growth factor-β1 and *Wnt*, which could explain this beneficial effect.[51]

Muscular regenerative capacities are also hindered in aged muscle tissue; thus, we transplanted muscle tissue of aged null and s-KL treated animals (24 MO) into young healthy recipients. This process simulates a strong muscular injury allowing the study of muscular regenerative capacities of treated mice. Interestingly, grafted tissue from animals treated with s-KL vectors was composed of muscle fibers presenting a larger average size, being similar to the muscular composition of young animals.[47] Moreover, an increase in the number of satellite cells and induction of new muscular cells generation was observed in the grafts, demonstrated by an increased number of $PAX7^+/Ki67^+$ and $MyoD^+/Ki67^+$ cells, respectively. These results agree with previous reports showing a clear link between KL and muscle regeneration, which is attributed to the preservation of mitochondrial microstructure in muscle stem cells.[52] Moreover, KL is also involved in the regulation of aberrant *Wnt* signaling in aged muscle stem cells, promoting its functionality.[53,54] Further research is required to elucidate the mechanism of action of s-KL to promote muscle regeneration after muscle transplantation.

Bone tissue is also highly affected during aging, associated with alterations in bone microarchitecture and a decrease in bone mineral density. Here, AAV9 administration efficiently increased basal levels of s-KL expression in the bone, which similar to previous reports did not generate toxic effects on this tissue.[27] At the endpoint of the experiment, females treated with s-KL at 6 months and males treated at 12 months of age, presented greater trabecular bone volume, trabecular number and thickness, and reduced trabecular space, reaching statistical significance in females. Females begin trabecular degeneration earlier than males. Therefore, the systemic increase in s-KL levels in females treated at 6 MO presents therapeutic benefits, which are not seen when trabecular degeneration is already advanced (treatment at 12 MO). In contrast, the higher s-KL concentration observed in males treated at 12 MO, a period when trabecular degeneration is pronounced in males, seems to be more effective in preserving trabecular bone.[55]

Gene expression analysis of bones from aged C57BL/6J treated with KL revealed an increase in the expression of genes like *Col1a1* and *Bglap*, reaching statistical significance in females. These transcripts encode the main structural protein component and a protein involved in regulating Ca^{2+} ion concentration in bones, respectively, suggesting increased bone formation and/or maintenance.[56] This could represent a possible mechanism to explain trabecular bone improvements seen in this model after the treatment with the s-KL isoform. Several studies have reported a positive effect of KL in maintaining bone microstructure and protecting its composition under normal and disease conditions.[57–59] Moreover, KL regulates the expression of non-collagenous bone proteins, like osteocalcin (BGLAP) and DMP-1, which are altered in the KL-knockout (KL-KO) model and provoke deficient bone calcification and osteoblast differentiation.[60] Interestingly, *in vitro* cultured osteoblasts treated with soluble KL increased several bone morphogenic proteins, including BGLAP, due to a KL-dependent activation of epidermal growth factor-1 signaling.[61] Additionally, a significant increase in *Runx2* gene expression was detected in s-KL-treated female mice. *Runx2* is a transcription factor associated with osteoblast differentiation, whose expression is reduced during aging.[62,63] This effect, together with the enhanced expression of bone morphogenic proteins, could indicate increased bone formation in s-KL-treated females. Finally, a reduction of *Fgf23* gene expression in s-KL-treated females was observed. Previous reports showed an age-associated increase in *Fgf23* expression, which was related to an impairment in bone mineralization, specifically in females.[64] This trend could be inhibited in s-KL-treated mice, promoting bone preservation. Therefore, mice treated with s-KL improved microstructure parameters altered during osteoporosis progression, especially

Figure 6. Transcriptomic analysis of hippocampal RNA-seq data

(A) Principal component analysis (PCA) showing overall gene expression patterns in null young (5 MO), null old (24 MO), and s-KL old (24 MO) male mice; $n = 4–5$. (B) Venn diagram showing the number of shared DEGs between the different male mice groups. (C) Bar chart presenting the pathway enrichment analysis of DEGs. (D) Schematic representation of the altered pathways' activation and the main molecules driving these changes.

females treated at 6 MO. This could be explained by an increase in the expression of bone morphogenic proteins and promoting osteoblast maturation. Further research is needed to elucidate the underlying mechanisms by which s-KL is improving the aging phenotype of bone tissue in treated mice.

KL was also effective in promoting cognition and protecting against dementia, modulating several pathways altered during aging, for instance modulating adult neurogenesis and regulating inflammation in the CNS.[65,66] Transgenic mice constitutively over-expressing KL exhibit increased markers for adult neurogenesis and increased dendritic arborization, while young KL-KO mice experience early stem cell reservoir depletion.[65,67] In the animals treated with s-KL at 12 MO, we detected a significant increase in the number of maturing neurons (DCX^+ cells), which are highly reduced during senescence, and a tendency to an increased thickness of the DG granular layer. This effect was also observed in healthy young mice treated with s-KL, where we observed an increase in both the number of neuronal stem cells ($Ki67^+$ cells), and in the number of DCX^+ cells. This result shows the s-KL effect in promoting and maintaining adult neurogenesis in wild-type animals. This cognition-enhancing property could be mediated by KL-dependent inhibition of the *Wnt* pathway, previously linked to stem cell niche maintenance, and/or be an indirect consequence of a reduction in age-associated stressor factors like oxidative or inflammatory stress after KL treatment, allowing for proper neuronal maturation.[68]

During aging there is a progressive accumulation of senescent cells and cellular debris, which can induce chronic pro-inflammatory responses driven by microglia and astrocytes, generating neuronal damage. Additionally, a loss in microglia and astrocytes number and arborization has been reported, causing a decrease in the functions performed by these cells.[17,69,70] Here, long-term s-KL-treated mice presented an increased number of $GFAP^+$ cells at both administration points compared with aged null-treated mice. Interestingly, the number of $GFAP^+$ cells reached values comparable with those observed in young null-treated animals, suggesting that the s-KL treatment may help to maintain astrocyte levels like those in healthy animals. Similarly, a decrease in $GFAP^+$ cells was detected in the hippocampus of the accelerated-aging SAMP8 model, correlating with a decline in the neurogenic niche.[71] This loss in $GFAP^+$ cells in the dentate gyrus was reverted in s-KL-treated SAMP8 mice.[72]

Chronic activation of microglial cells, a state known as reactive microgliosis, compromises phagocytosis and increases the secretion of pro-inflammatory cytokines.[19,20] Previous studies have shown that KL reduces inflammatory stress in the aging CNS,[73] while KL depletion contributes to increased inflammation in mice,[74] suggesting KL therapeutical potential to reduce inflammaging and protect neurons.[75–77] In this study, animals treated with s-KL at the 12 MO time point, where the most beneficial effects were observed, presented an increased number of $Iba1^+$ cells compared with null-treated animals. In contrast, young healthy animals treated with s-KL did not exhibit an increase in the number of $Iba1^+$ nor $GFAP^+$ cells, suggesting this effect is just observed in aged brains.

To better understand these changes, we performed an RNA-seq analysis of the hippocampus from young and aged mice treated with s-KL or null vectors. Comparing the transcription profile of young and aged animals treated with null vectors, which would represent non-pathological aging progression, we observed decreased activation of canonical pathways involved in oxidative phosphorylation and increased mitochondrial dysfunction, typical aging hallmarks.[78] In contrast, compared with young null mice, aged animals treated with s-KL presented increased signaling and activation of immune cells, but not other aging hallmarks, indicating that s-KL expression modulates the transcriptional landscape of the hippocampus during aging. On the other hand, comparing the transcriptome of 24-MO male mice treated with null, or s-KL at the 12 MO time point, which presented the higher aging phenotypical improvement, the top enriched pathways were involved in (1) phagocytosis promotion, (2) immune cell activation and mobilization, and (3) decreased pro-inflammatory responses. Therefore, the increase in $Iba1^+$ cells observed after s-KL treatment in 12 MO animals seems to be accompanied by an induction of phagocytic responses and a decrease in pro-inflammatory signaling in the hippocampus, previously described as well-functioning microglial functions.[79] Thus, the enhanced cognitive capacity observed in previous experiments after s-KL expression in aged CNS could be due, at least in part, to the promotion of clearance of malfunctioning proteins and senescent cells, benefiting adult neurogenesis.[72,80] More research is needed to fully understand the s-KL mechanism underlying the increase in $Iba1^+$ cell number and phagocytosis activity.

In summary, here we show the therapeutic effects of exogenous lifelong overexpression of s-KL in wild-type mice. Of note, s-KL induced multiple beneficial effects which synergically led to an increase in total longevity, improving physical state, muscle tissue integrity and regenerative capacity. Moreover, it also improved trabecular bone parameters affected during aging. Finally, s-KL partially recapitulated the increased neurogenesis levels observed in the KL-OE mice model, promoted maintenance in astrocyte cell numbers, and increased the phagocytic capacity of microglia.

METHODS

Animal housing

Six-week-old male and female C57BL/6J mice were purchased from Charles River Labs. A cohort of 96 animals was divided into three groups. Two groups were treated when they were in a young-adult developmental stage (6 MO) with a AAV9-null (no transcribing vector) or AAV9-s-KL. The third group was treated with an AAV9-s-KL when animals were adults (12 MO). Animals had free access to food and water and were kept under standard temperature conditions (22 ± 2°C) and a 12-h light/dark cycle (300 lux/0 lux).

All experimental procedures involving animals were performed following standard ethical guidelines of the European Communities Council Directive 86/609/EEC and by the Institutional Animal Care and Use Committee of the Universitat Autònoma de Barcelona (M0348-DO5, procedure code P1- 4882).

AAV vector production and administration

AAV9 were generated in HEK293 cells by the triple transfection method at the Unitat de Producció de Vectors at Universitat Autònoma de Barcelona following a protocol described previously.[81] Briefly, viral vectors were precipitated using a hypersaline solution and treated with Benzonase (Novagen), followed by purification with an iodixanol density gradient (Axis-Shield PoC AS) separated by ultracentrifugation. Vector concentration was quantified using the Picogreen method (Invitrogen).

AAV9s were administered by simultaneous ICV and IV injection. Animals were deeply anesthetized by intraperitoneal injection of 10 mg/kg of ketamine (Imalgene 500, Rhone-Merieux) and 1 mg/kg of xylazine (Rompun, Bayer) diluted in NaCl 0.9%. Stereotaxic injections were performed at coordinates, −0.2 mm anteroposterior, −2 mm dorsoventral, and +1 mm mediolateral from bregma. The vector dose was 1×10^{11} viral genomes per animal in 6 μL, administered at a 0.5 μL/min using an ultramicropump (WorldPrecision Instruments). The IV injection consisted in a dose of 4×10^{11} viral genomes per animal diluted with NaCl 0.9% to a final volume of 200 μL and injected manually with a syringe into the lateral tail vein of the mice.

Longevity follow-up

Mice were periodically monitored to assess their general health status and body weight. During the first year, the animals were reviewed every 3 months. In the second year, the animals were examined monthly, and after reaching 2 years of age, they were checked weekly. The follow-up of the animals was conducted until natural death or euthanasia, as determined by a blinded veterinarian, occurred.

Behavioral tests

Behavioral tests were done on all animals at the age of 24 MO to assess physical status. These tests included the horizontal wooden bar, rotarod, and grip strength.

Horizontal wooden bar

A circular wooden bar with a diameter of 1 cm , was horizontally placed 40 cm above a soft floor made of expanded polystyrene. Mice were carefully suspended on the bar by their upper limbs, a maximum test length of 40 s. Time spent on the bar (resistance) and distance walked along the bar (coordination), were recorded. Two trials per animal were done, and the best performance was selected.

Rotarod

Animals were trained in the rotarod apparatus for 3 consecutive days. Training consisted in two accelerated rotarod test trials per day to reduce stress and improve coordination, facilitating the differences observation due exclusively to physical state limitations. Experimental conditions consisted in a 5 min long test with progressive acceleration from 4 to 40 rpm. The day of the test, animals were carefully placed in a previously cleaned rotarod apparatus, and the time to fall was quantified. The test was done twice, and the represented results are the average of both trials per animal.

Grip strength

Grip strength was measured as tension force using a computerized force transducer, Grip Strength Meter (Bioseb). Animals were let to grip from the front legs to the grip strength platform and were pulled backwards from the tail slowly so the animal could present resistance, until reaching the end of the platform. This procedure was repeated three times and data are presented as each group's average strength by trial allowing the observation of the exhaustion effect in the animals.

Sample harvest

Animals were euthanized by cervical dislocation 3 days after the last behavioral test. Perfusions were done with deeply anesthetized animals with 1 mL of ketamine (100 mg/mL) (Imalgene) and 0.5 mL of xylazine (Rompun) in 1× PBS up to 10 mL, and the procedure was started when animals presented no pedal reflex. The hippocampus and cortex were then isolated and frozen in powdered dry ice. Liver, muscle, and bone samples were also taken, and they were maintained at −80°C until used for molecular analysis or fixed in a 4% PFA in 1× PBS if they were used for morphological analysis.

ELISA

KL serum levels were measured using an ELISA kit specific for mouse KL (IBL) following manufacturers' indications. For this assay, a dilution of 1:20 of the serum was used and absorbance at 450 nm was read with a plate reader Varioskan LUX VLBL00D0 (Thermo Fisher Scientific) at the Laboratori de Biologia Molecular of the Institut de Neurociències at the UAB.

RNA extraction and gene expression analysis

Total RNA isolation was carried out using TRIsure reagent following the manufacturer's instructions (Bioline Reagent). The liver or tibia samples were homogenized using TissueLyser LT sample disruption apparatus (QIAGEN). RNA quantity and purity were measured with NanoDrop 1000 Spectrophotometer (Thermo Fisher Scientific). RNA retrotranscription was done using iScript Advanced cDNA Synthesis Kit (Bio-Rad). Gene expression was analyzed by real-time qPCR on a Bio-Rad CFX-384 PCR machine at the Analysis and Photodocumentation Service of the Universitat Autonòma de Barcelona. In case of TaqMan probes, each reaction contained 5 μL of Sensifast probe No-Rox master mix (Meridian Bioscience), 0.5 μL TaqMan mix (ThermoFisher scientific) and H_2O to a final volume of 10 μL were used. TaqMan probes used are listed in Table S3. Custom TaqMan probes (CondaLab) used were: m36b4 (Rplp0)

(forward: 5′-ATGGGTACAAGCGCGTCCTG-3′; reverse: 5′-AGC CGCAAATGCAGATGGATC-3′; probe: 5′-TGTGGAGACTGAGT ACACCTTCCCA-3′) and s-KL (forward: 5′-TCATAATGGAAA CCTTAAAAGCAA-3′; reverse: 5′-CACTGGGTTTTGTCAAAG GA-3′; probe: 5′-AGAAGAGTCCTCGCCGGATGCTGTA-3′).

The analysis of qPCR data was done following the ΔΔCt method. Cycle thresholds (Cqs) were normalized subtracting to each experimental Cq, the difference of its housekeeping (HK) Cq compared with the HK's average value. HK genes used were m36b4 (vector expression) and Tbp (bone gene expression). Melting curves were also analyzed to ensure unique amplificon generation.

Histology

Animals were intracardially perfused with a cold PBS solution. Samples were then dissected and submerged in PFA 4% for 24 h. Samples were washed using PBS and then incubated in 30% sucrose at 4°C for cryoprotection.

Muscle slices of 10 μm were stained for hematoxylin and eosin or Sirius red (Sigma-Aldrich) following commercial protocols. Muscle fiber size and percentage of area positive for Sirius red staining were quantified using ImageJ software. Digital images were acquired using the Leica DMR600B microscope equipped with a DFC300FX camera.

For free-floating immunohistochemistry, samples were frozen by 1.5 min submersion in Isopentane (Sigma) at −40°C to −60°C. Coronal sections of 30 μm were cut using a cryostat and stored submerged in cryoprotectant solution at −20°C. For staining, sections were washed with incubations in 1× PBS and permeabilized in 0.2% PBS-Triton buffer, followed by a 1-h blocking with 10% BSA in 1× PBS with 0.2% Triton. Incubation of the primary antibody was performed at 4°C for 48 h, and with secondary antibody was performed at 4°C overnight. Finally, a 5-min incubation with Hoechst was done and samples were mounted with fFluoromount. The antibodies used for the analysis can be found in Table S4.

Images were obtained with a Zeiss LSM880 high-speed spectral confocal microscope. Images were analyzed with ImageJ software and Imaris Microscopy Image Analysis Software.

Muscle grafting

Heterografting experiments were performed by removing the extensor digitorum longus muscle from 24 MO treated mice from its anatomical bed and transplanting it onto the surface of the tibialis anterior muscle of a young (3 MO) WT recipient mouse. Muscle grafts were collected for analysis on day 7 after transplantation to assess the regenerative state of the tissue.

Bone structural study

Right legs of treated animals were analyzed as previously described.[72] Briefly, tibias from treated animals euthanized at the age of 24 ± 3 MO were dissected and scanned using a SkyScan 1272 (Bruker) computerized microtomography imaging system at the Center de Recerca en Ciència i Enginyeria Multiescala de Barcelona at Universitat Politècnica de Catalunya. Images were reconstructed with the NRecon v1.6 (Bruker) program and analyzed with the CT-Analyser v1.13 image program (Bruker). Mineral density was calculated with the CT-Analyzer v1.13 program calibrating bone absorbance with two 2mm diameter hydroxyapatite phantoms (Bruker-MicroCT) of known density of 0.25 and 0.75 g/cm^3.

RNA-seq

Total hippocampus RNA was extracted using the RNeasy Plus RNA extraction kit (QIAGEN), which allowed specific isolation of total RNA molecules, excluding genomic DNA. RNA quantity and quality was assessed by Bioanalyzer (Agilent) in the Center for Genomic Regulation facilities of the Barcelona Biomedical Research Park. Libraries were prepared using the TruSeq stranded mRNA Library Prep (Illumina) according to the manufacturers' protocol, to convert total RNA into a library of template molecules of known strand origin and suitable for subsequent cluster generation and DNA sequencing. Then, RNA fragments were copied into cDNA using reverse transcriptase SuperScript II (Invitrogen) and random primers. Subsequent ligation of the multiple indexing adapter to the ends of the double stranded cDNA was done. Finally, PCR selectively enriched those DNA fragments that had adapter molecules on both ends. The PCR was performed with a PCR Primer Cocktail that anneals to the ends of the adapters. Final libraries were analyzed using Bioanalyzer DNA 1000 or Fragment Analyzer Standard Sensitivity (Agilent) to estimate the quantity and validate the size distribution and were then quantified by qPCR using the KAPA Library Quantification Kit KK4835 (Roche) before the amplification with Illumina's cBot. Libraries were sequenced twice 50 + 8 + 8 bp on Illumina's NextSeq2000 sequencer.

Bioinformatic analysis consisted of several steps. First, RNA-seq reads were trimmed, to eliminate the possible adapter sequences present in the reads and aligned to the *Mus musculus* reference genome. With this, raw counts were obtained, which were next normalized, grouped and compared with other samples using the DEseq2 script coded in R. This gave us the DEGs, with a statistical significance analysis. DEGs which presented a P-adjusted value lower than 0.05 were introduced into the Ingenuity Pathway Analysis program (QIAGEN), which interpreted the data and listed the different altered pathways after the treatment and pointed out their possible biological implications. Canonical pathways showed by statistical significance, fold change, and biological significance.

Statistical analysis

Statistical analysis and graphic representation were done with GraphPad Prism ver.8 (GraphPad Software). Statistical differences between groups were analyzed with a two-tailed unpaired Student's t test when comparing two groups, and one-way ANOVA, followed by Tukey as a *post hoc* analysis when it was necessary. Data are expressed as mean ± SEM. Statistical difference was accepted when p values were less than or equal to 0.05 and outliers were detected by

Grubb's test and removed from the analysis. The graphical abstract and Figure 1 were created with BioRender.com.

DATA AVAILABILITY

Data that support the findings of this study are available from the corresponding author upon reasonable request.

ACKNOWLEDGMENTS

This work was financed by MICINN/AEI/10.13039/501100011033 (PID2022-14624OB-100 and PID2019-104034RB-100 to M.C.) and (PID2023-148834OB-I00) to A.B.; by the Instituto de Salud Carlos III and NexGenerationEU (RICORS, RD21/0017/0008) to M.C. and A.B.; and Generalitat de Catalunya (2021SGR-00529) to A.B. and M.C.

AUTHOR CONTRIBUTIONS

J.R.S., Á.E., S.V., C.M.A., L.R.E., A.L.S., and B.A.J. conducted the experiments; J.R.S., C.S.D., B.A.J., P.M.C., and M.C. designed the experiments; J.R.S., C.R.A., C.S.D., A.B., F.V., B.A.J., P.M.C., and M.C. performed the formal analysis; J.R.S. and M.C. wrote the paper; all authors reviewed and edited the paper.

DECLARATION OF INTERESTS

Portions of this work are the subject of patent applications held by the Universitat Autonoma de Barcelona (UAB, Spain); the Universitatde Barcelona (UB, Spain); the Institucio Catalana de Recerca i Estudis Avançats (ICREA, Spain); and the Vall d'Hebron Institute of Research (VHIR, Spain). J.R.S., A.B., M.C., A.L.S. and P.M., are included in these patent applications. M.C.R. is scientific advisor of ANEW medical, a company that is seeking to develop KL-boosting therapeutics.

SUPPLEMENTAL INFORMATION

Supplemental information can be found online at https://doi.org/10.1016/j.ymthe.2025.02.030.

REFERENCES

1. Cristea, M., Noja, G.G., Stefea, P., and Sala, A.L. (2020). The Impact of Population Aging and Public Health Support on EU Labor Markets. Int. J. Environ. Res. Public Health *17*, 1439.
2. Sorond, F.A., Cruz-Almeida, Y., Clark, D.J., Viswanathan, A., Scherzer, C.R., De Jager, P., Csiszar, A., Laurienti, P.J., Hausdorff, J.M., Chen, W.G., et al. (2015). Aging, the Central Nervous System, and Mobility in Older Adults: Neural Mechanisms of Mobility Impairment. J. Gerontol. A. Biol. Sci. Med. Sci. *70*, 1526–1532.
3. Hughes, V.A., Frontera, W.R., Wood, M., Evans, W.J., Dallal, G.E., Roubenoff, R., and Fiatarone Singh, M.A. (2001). Longitudinal muscle strength changes in older adults: influence of muscle mass, physical activity, and health. J. Gerontol. A. Biol. Sci. Med. Sci. *56*, B209–B217.
4. Volpi, E., Nazemi, R., and Fujita, S. (2004). Muscle tissue changes with aging. Curr. Opin. Clin. Nutr. Metab. Care *7*, 405–410.
5. Siparsky, P.N., Kirkendall, D.T., and Garrett, W.E., Jr. (2014). Muscle changes in aging: understanding sarcopenia. Sports Health *6*, 36–40.
6. Mann, C.J., Perdiguero, E., Kharraz, Y., Aguilar, S., Pessina, P., Serrano, A.L., and Muñoz-Cánoves, P. (2011). Aberrant repair and fibrosis development in skeletal muscle. Skelet. Muscle *1*, 21.
7. Hong, X., Isern, J., Campanario, S., Perdiguero, E., Ramírez-Pardo, I., Segalés, J., Hernansanz-Agustín, P., Curtabbi, A., Deryagin, O., Pollán, A., et al. (2022). Mitochondrial dynamics maintain muscle stem cell regenerative competence throughout adult life by regulating metabolism and mitophagy. Cell Stem Cell *29*, 1506–1508.
8. Glass, D.J. (2023). Senescent cells damage the body throughout life. Nature *613*, 30–31.
9. Riggs, B.L., Melton Iii, L.J., 3rd, Robb, R.A., Camp, J.J., Atkinson, E.J., Peterson, J.M., Rouleau, P.A., McCollough, C.H., Bouxsein, M.L., and Khosla, S. (2004). Population-based study of age and sex differences in bone volumetric density, size, geometry, and structure at different skeletal sites. J. Bone Miner. Res. *19*, 1945–1954.
10. Ferguson, V.L., Ayers, R.A., Bateman, T.A., and Simske, S.J. (2003). Bone development and age-related bone loss in male C57BL/6J mice. Bone *33*, 387–398.
11. Mosekilde, L., and Mosekilde, L. (1990). Sex differences in age-related changes in vertebral body size, density and biomechanical competence in normal individuals. Bone *11*, 67–73.
12. Corrado, A., Cici, D., Rotondo, C., Maruotti, N., and Cantatore, F.P. (2020). Molecular Basis of Bone Aging. Int. J. Mol. Sci. *21*, 3679.
13. Licini, C., Vitale-Brovarone, C., and Mattioli-Belmonte, M. (2019). Collagen and non-collagenous proteins molecular crosstalk in the pathophysiology of osteoporosis. Cytokine Growth Factor Rev. *49*, 59–69.
14. Hampel, H., and Lista, S. (2016). Dementia: The rising global tide of cognitive impairment. Nat. Rev. Neurol. *12*, 131–132.
15. Leal-Galicia, P., Chavez-Hernandez, M.E., Mata, F., Mata-Luevanos, J., Rodriguez-Serrano, L.M., Tapia-de-Jesus, A., and Buenrostro-Jauregui, M.H. (2021). Adult Neurogenesis: A Story Ranging from Controversial New Neurogenic Areas and Human Adult Neurogenesis to Molecular Regulation. Int. J. Mol. Sci. *22*, 11489.
16. Sikora, E., Bielak-Zmijewska, A., Dudkowska, M., Krzystyniak, A., Mosieniak, G., Wesierska, M., and Wlodarczyk, J. (2021). Cellular Senescence in Brain Aging. Front. Aging Neurosci. *13*, 646924.
17. Zoller, T., Attaai, A., Potru, P.S., Russ, T., and Spittau, B. (2018). Aged Mouse Cortical Microglia Display an Activation Profile Suggesting Immunotolerogenic Functions. Int. J. Mol. Sci. *19*, 706.
18. Matias, I., Morgado, J., and Gomes, F.C.A. (2019). Astrocyte Heterogeneity: Impact to Brain Aging and Disease. Front. Aging Neurosci. *11*, 59.
19. Swenson, B.L., Meyer, C.F., Bussian, T.J., and Baker, D.J. (2019). Senescence in aging and disorders of the central nervous system. Translational Med. Aging *3*, 17–25.
20. Galloway, D.A., Phillips, A.E.M., Owen, D.R.J., and Moore, C.S. (2019). Phagocytosis in the Brain: Homeostasis and Disease. Front. Immunol. *10*, 790.
21. Chen, C.D., Tung, T.Y., Liang, J., Zeldich, E., Tucker Zhou, T.B., Turk, B.E., and Abraham, C.R. (2014). Identification of cleavage sites leading to the shed form of the anti-aging protein klotho. Biochemistry *53*, 5579–5587.
22. Kuro-o, M., Matsumura, Y., Aizawa, H., Kawaguchi, H., Suga, T., Utsugi, T., Ohyama, Y., Kurabayashi, M., Kaname, T., Kume, E., et al. (1997). Mutation of the mouse klotho gene leads to a syndrome resembling ageing. Nature *390*, 45–51.
23. Shiraki-Iida, T., Aizawa, H., Matsumura, Y., Sekine, S., Iida, A., Anazawa, H., Nagai, R., Kuro-o, M., and Nabeshima, Y. (1998). Structure of the mouse klotho gene and its two transcripts encoding membrane and secreted protein. FEBS Lett. *424*, 6–10.
24. Chen, G., Liu, Y., Goetz, R., Fu, L., Jayaraman, S., Hu, M.C., Moe, O.W., Liang, G., Li, X., and Mohammadi, M. (2018). alpha-Klotho is a non-enzymatic molecular scaffold for FGF23 hormone signalling. Nature *553*, 461–466.
25. Kurosu, H., Ogawa, Y., Miyoshi, M., Yamamoto, M., Nandi, A., Rosenblatt, K.P., Baum, M.G., Schiavi, S., Hu, M.C., Moe, O.W., and Kuro-o, M. (2006). Regulation of fibroblast growth factor-23 signaling by klotho. J. Biol. Chem. *281*, 6120–6123.
26. Abraham, C.R., and Li, A. (2022). Aging-suppressor Klotho: Prospects in diagnostics and therapeutics. Ageing Res. Rev. *82*, 101766.
27. Roig-Soriano, J., Sánchez-de-Diego, C., Esandi-Jauregui, J., Verdés, S., Abraham, C.R., Bosch, A., Ventura, F., and Chillón, M. (2023). Differential toxicity profile of secreted and processed alpha-Klotho expression over mineral metabolism and bone microstructure. Sci. Rep. *13*, 4211.
28. Jaijyan, D.K., Selariu, A., Cruz-Cosme, R., Tong, M., Yang, S., Stefa, A., Kekich, D., Sadoshima, J., Herbig, U., Tang, Q., et al. (2022). New intranasal and injectable gene therapy for healthy life extension. Proc. Natl. Acad. Sci. USA *119*, e2121499119.
29. Davidsohn, N., Pezone, M., Vernet, A., Graveline, A., Oliver, D., Slomovic, S., Punthambaker, S., Sun, X., Liao, R., Bonventre, J.V., and Church, G.M. (2019). A single combination gene therapy treats multiple age-related diseases. Proc. Natl. Acad. Sci. USA *116*, 23505–23511.
30. Senis, E., Mosteiro, L., Wilkening, S., Wiedtke, E., Nowrouzi, A., Afzal, S., Fronza, R., Landerer, H., Abad, M., Niopek, D., et al. (2018). AAVvector-mediated in vivo reprogramming into pluripotency. Nat. Commun. *9*, 2651.

31. Bernardes de Jesus, B., Vera, E., Schneeberger, K., Tejera, A.M., Ayuso, E., Bosch, F., and Blasco, M.A. (2012). Telomerase gene therapy in adult and old mice delays aging and increases longevity without increasing cancer. EMBO Mol. Med. *4*, 691–704.

32. Zincarelli, C., Soltys, S., Rengo, G., and Rabinowitz, J.E. (2008). Analysis of AAV serotypes 1-9 mediated gene expression and tropism in mice after systemic injection. Mol. Ther. *16*, 1073–1080.

33. Leon, J., Moreno, A.J., Garay, B.I., Chalkley, R.J., Burlingame, A.L., Wang, D., and Dubal, D.B. (2017). Peripheral Elevation of a Klotho Fragment Enhances Brain Function and Resilience in Young, Aging, and alpha-Synuclein Transgenic Mice. Cell Rep. *20*, 1360–1371.

34. Rocca, C.J., Ur, S.N., Harrison, F., and Cherqui, S. (2014). rAAV9 combined with renal vein injection is optimal for kidney-targeted gene delivery: conclusion of a comparative study. Gene Ther. *21*, 618–628.

35. Castle, M.J., Turunen, H.T., Vandenberghe, L.H., and Wolfe, J.H. (2016). Controlling AAV Tropism in the Nervous System with Natural and Engineered Capsids. Methods Mol. Biol. *1382*, 133–149.

36. Nonnenmacher, M., Wang, W., Child, M.A., Ren, X.Q., Huang, C., Ren, A.Z., Tocci, J., Chen, Q., Bittner, K., Tyson, K., et al. (2021). Rapid evolution of blood-brain-barrier-penetrating AAV capsids by RNA-driven biopanning. Mol. Ther. Methods Clin. Dev. *20*, 366–378.

37. Dou, Y., Lin, Y., Wang, T.Y., Wang, X.Y., Jia, Y.L., and Zhao, C.P. (2021). The CAG promoter maintains high-level transgene expression in HEK293 cells. FEBS Open Bio *11*, 95–104.

38. Dutta, S., and Sengupta, P. (2016). Men and mice: Relating their ages. Life Sci. *152*, 244–248.

39. Flurkey, M., Currer, J., and Harrison, D. (2007). The mouse in biomedical research. Chapt. 20 - Mouse Models in Aging Research. Am. Coll. Lab. Anim. Med. *III*, 637–672.

40. Torres-Torronteras, J., Cabrera-Pérez, R., Vila-Julià, F., Viscomi, C., Cámara, Y., Hirano, M., Zeviani, M., and Martí, R. (2018). Long-Term Sustained Effect of Liver-Targeted Adeno-Associated Virus Gene Therapy for Mitochondrial Neurogastrointestinal Encephalomyopathy. Hum. Gene Ther. *29*, 708–718.

41. Davidoff, A.M., Ng, C.Y.C., Zhou, J., Spence, Y., and Nathwani, A.C. (2003). Sex significantly influences transduction of murine liver by recombinant adeno-associated viral vectors through an androgen-dependent pathway. Blood *102*, 480–488.

42. Hampton, A.L., Hish, G.A., Aslam, M.N., Rothman, E.D., Bergin, I.L., Patterson, K.A., Naik, M., Paruchuri, T., Varani, J., and Rush, H.G. (2012). Progression of ulcerative dermatitis lesions in C57BL/6Crl mice and the development of a scoring system for dermatitis lesions. J. Am. Assoc. Lab. Anim. Sci. *51*, 586–593.

43. Kurosu, H., Yamamoto, M., Clark, J.D., Pastor, J.V., Nandi, A., Gurnani, P., McGuinness, O.P., Chikuda, H., Yamaguchi, M., Kawaguchi, H., et al. (2005). Suppression of aging in mice by the hormone Klotho. Science *309*, 1829–1833.

44. Dubal, D.B., Yokoyama, J.S., Zhu, L., Broestl, L., Worden, K., Wang, D., Sturm, V.E., Kim, D., Klein, E., Yu, G.Q., et al. (2014). Life extension factor klotho enhances cognition. Cell Rep. *7*, 1065–1076.

45. Ge, X., Cho, A., Ciol, M.A., Pettan-Brewer, C., Snyder, J., Rabinovitch, P., and Ladiges, W. (2016). Grip strength is potentially an early indicator of age-related decline in mice. Pathobiol. Aging Age Relat. Dis. *6*, 32981.

46. Della Peruta, C., Lozanoska-Ochser, B., Renzini, A., Moresi, V., Sanchez Riera, C., Bouché, M., and Coletti, D. (2023). Sex Differences in Inflammation and Muscle Wasting in Aging and Disease. Int. J. Mol. Sci. *24*, 4651.

47. Uchitomi, R., Hatazawa, Y., Senoo, N., Yoshioka, K., Fujita, M., Shimizu, T., Miura, S., Ono, Y., and Kamei, Y. (2019). Metabolomic Analysis of Skeletal Muscle in Aged Mice. Sci. Rep. *9*, 10425.

48. Shavlakadze, T., McGeachie, J., and Grounds, M.D. (2010). Delayed but excellent myogenic stem cell response of regenerating geriatric skeletal muscles in mice. Biogerontology *11*, 363–376.

49. Clemens, Z., Sivakumar, S., Pius, A., Sahu, A., Shinde, S., Mamiya, H., Luketich, N., Cui, J., Dixit, P., Hoeck, J.D., et al. (2021). The biphasic and age-dependent impact of klotho on hallmarks of aging and skeletal muscle function. Elife *10*, e61138.

50. Moiseeva, V., Cisneros, A., Sica, V., Deryagin, O., Lai, Y., Jung, S., Andrés, E., An, J., Segalés, J., Ortet, L., et al. (2023). Senescence atlas reveals an aged-like inflamed niche that blunts muscle regeneration. Nature *613*, 169–178.

51. Phelps, M., Pettan-Brewer, C., Ladiges, W., and Yablonka-Reuveni, Z. (2013). Decline in muscle strength and running endurance in klotho deficient C57BL/6 mice. Biogerontology *14*, 729–739.

52. Sahu, A., Mamiya, H., Shinde, S.N., Cheikhi, A., Winter, L.L., Vo, N.V., Stolz, D., Roginskaya, V., Tang, W.Y., St Croix, C., et al. (2018). Age-related declines in alpha-Klotho drive progenitor cell mitochondrial dysfunction and impaired muscle regeneration. Nat. Commun. *9*, 4859.

53. Ahrens, H.E., Huettemeister, J., Schmidt, M., Kaether, C., and von Maltzahn, J. (2018). Klotho expression is a prerequisite for proper muscle stem cell function and regeneration of skeletal muscle. Skelet. Muscle *8*, 20.

54. Welc, S.S., Wehling-Henricks, M., Kuro-O, M., Thomas, K.A., and Tidball, J.G. (2020). Modulation of Klotho expression in injured muscle perturbs Wnt signalling and influences the rate of muscle growth. Exp. Physiol. *105*, 132–147.

55. Glatt, V., Canalis, E., Stadmeyer, L., and Bouxsein, M.L. (2007). Age-related changes in trabecular architecture differ in female and male C57BL/6J mice. J. Bone Miner. Res. *22*, 1197–1207.

56. Di Medio, L., and Brandi, M.L. (2021). Advances in bone turnover markers. Adv. Clin. Chem. *105*, 101–140.

57. Suzuki, H., Amizuka, N., Oda, K., Noda, M., Ohshima, H., and Maeda, T. (2008). Histological and elemental analyses of impaired bone mineralization in klotho-deficient mice. J. Anat. *212*, 275–285.

58. Maruyama, N., Shibata, Y., Mochizuki, A., Yamada, A., Maki, K., Inoue, T., Kamijo, R., and Miyazaki, T. (2015). Bone micro-fragility caused by the mimetic aging processes in alpha-klotho deficient mice: in situ nanoindentation assessment of dilatational bands. Biomaterials *47*, 62–71.

59. Lin, W., Li, Y., Chen, F., Yin, S., Liu, Z., and Cao, W. (2017). Klotho preservation via histone deacetylase inhibition attenuates chronic kidney disease-associated bone injury in mice. Sci. Rep. *7*, 46195.

60. Sasaki, M., Hasegawa, T., Yamada, T., Hongo, H., de Freitas, P.H.L., Suzuki, R., Yamamoto, T., Tabata, C., Toyosawa, S., Yamamoto, T., et al. (2013). Altered distribution of bone matrix proteins and defective bone mineralization in klotho-deficient mice. Bone *57*, 206–219.

61. Toan, N.K., Tai, N.C., Kim, S.A., and Ahn, S.G. (2020). Soluble Klotho regulates bone differentiation by upregulating expression of the transcription factor EGR-1. FEBS Lett. *594*, 290–300.

62. Komori, T. (2008). Regulation of bone development and maintenance by Runx2. Front. Biosci. *13*, 898–903.

63. Becerikli, M., Jaurich, H., Schira, J., Schulte, M., Döbele, C., Wallner, C., Abraham, S., Wagner, J.M., Dadras, M., Kneser, U., et al. (2017). Age-dependent alterations in osteoblast and osteoclast activity in human cancellous bone. J. Cell. Mol. Med. *21*, 2773–2781.

64. Sirikul, W., Siri-Angkul, N., Chattipakorn, N., and Chattipakorn, S.C. (2022). Fibroblast Growth Factor 23 and Osteoporosis: Evidence from Bench to Bedside. Int. J. Mol. Sci. *23*, 2500.

65. Laszczyk, A.M., Fox-Quick, S., Vo, H.T., Nettles, D., Pugh, P.C., Overstreet-Wadiche, L., and King, G.D. (2017). Klotho regulates postnatal neurogenesis and protects against age-related spatial memory loss. Neurobiol. Aging *59*, 41–54.

66. Zhu, L., Stein, L.R., Kim, D., Ho, K., Yu, G.Q., Zhan, L., Larsson, T.E., and Mucke, L. (2018). Klotho controls the brain-immune system interface in the choroid plexus. Proc. Natl. Acad. Sci. USA *115*, E11388–E11396.

67. Salech, F., Varela-Nallar, L., Arredondo, S.B., Bustamante, D.B., Andaur, G.A., Cisneros, R., Ponce, D.P., Ayala, P., Inestrosa, N.C., Valdés, J.L., et al. (2019). Local Klotho Enhances Neuronal Progenitor Proliferation in the Adult Hippocampus. J. Gerontol. A. Biol. Sci. Med. Sci. *74*, 1043–1051.

68. Ullah, M., and Sun, Z. (2019). Klotho Deficiency Accelerates Stem Cells Aging by Impairing Telomerase Activity. J. Gerontol. A. Biol. Sci. Med. Sci. *74*, 1396–1407.

69. Fernandez, A., Quintana, E., Velasco, P., Moreno-Jimenez, B., de Andres, B., Gaspar, M.L., Liste, I., Vilar, M., Mira, H., and Cano, E. (2021). Senescent accelerated

prone 8 (SAMP8) mice as a model of age dependent neuroinflammation. J. Neuroinflammation *18*, 75.

70. Davies, D.S., Ma, J., Jegathees, T., and Goldsbury, C. (2017). Microglia show altered morphology and reduced arborization in human brain during aging and Alzheimer's disease. Brain Pathol. *27*, 795–808.

71. Gang, B., Yue, C., Han, N., Xue, H., Li, B., Sun, L., Li, X., and Zhao, Q. (2011). Limited hippocampal neurogenesis in SAMP8 mouse model of Alzheimer's disease. Brain Res. *1389*, 183–193.

72. Roig-Soriano, J., Grinan-Ferre, C., Espinosa-Parrilla, J.F., Abraham, C.R., Bosch, A., Pallas, M., and Chillon, M. (2022). AAV-mediated expression of secreted and transmembrane alphaKlotho isoforms rescues relevant aging hallmarks in senescent SAMP8 mice. Aging Cell *21*, e13581.

73. Maekawa, Y., Ishikawa, K., Yasuda, O., Oguro, R., Hanasaki, H., Kida, I., Takemura, Y., Ohishi, M., Katsuya, T., and Rakugi, H. (2009). Klotho suppresses TNF-alpha-induced expression of adhesion molecules in the endothelium and attenuates NF-kappaB activation. Endocrine *35*, 341–346.

74. Zhao, Y., Banerjee, S., Dey, N., LeJeune, W.S., Sarkar, P.S., Brobey, R., Rosenblatt, K.P., Tilton, R.G., and Choudhary, S. (2011). Klotho depletion contributes to increased inflammation in kidney of the db/db mouse model of diabetes via RelA (serine)536 phosphorylation. Diabetes *60*, 1907–1916.

75. Edler, M.K., Mhatre-Winters, I., and Richardson, J.R. (2021). Microglia in Aging and Alzheimer's Disease: A Comparative Species Review. Cells *10*, 1138.

76. Kinney, J.W., Bemiller, S.M., Murtishaw, A.S., Leisgang, A.M., Salazar, A.M., and Lamb, B.T. (2018). Inflammation as a central mechanism in Alzheimer's disease. Alzheimers Dement (N Y). *4*, 575–590.

77. Smith, K., and Semënov, M.V. (2019). The impact of age on number and distribution of proliferating cells in subgranular zone in adult mouse brain. IBRO Rep. *6*, 18–30.

78. Lopez-Otin, C., Blasco, M.A., Partridge, L., Serrano, M., and Kroemer, G. (2023). Hallmarks of aging: An expanding universe. Cell *186*, 243–278.

79. Gabande-Rodriguez, E., Keane, L., and Capasso, M. (2020). Microglial phagocytosis in aging and Alzheimer's disease. J. Neurosci. Res. *98*, 284–298.

80. Masso, A., Sanchez, A., Bosch, A., Gimenez-Llort, L., and Chillon, M. (2018). Secreted alphaKlotho isoform protects against age-dependent memory deficits. Mol. Psychiatry *23*, 1937–1947.

81. Piedra, J., Ontiveros, M., Miravet, S., Penalva, C., Monfar, M., and Chillon, M. (2015). Development of a rapid, robust, and universal picogreen-based method to titer adeno-associated vectors. Hum. Gene Ther. Methods *26*, 35–42.